On the detection of water vapor profiles and thin moisture layers from atmospheric radio occultations.

M. de la Torre Juárez

Jet Propulsion Laboratory/California Institute of Technology, 4800 Oak Grove Dr., Pasadena, CA 91109-8099, U.S.A.

M. Nilsson

Department of Radio and Space Science, Onsala Space Observatory, Chalmers University of Technology, Sweden.

Abstract. GPS radio occultations provide high-resolution vertical profiles of the atmospheric refraction index that can be used to extract vertical profiles of tropospheric moisture content. A physical method to extract water abundances from refraction index profiles without using ancillary data or model input is described. The ability to capture sharp water structures in the upper troposphere is illustrated by comparisons with current approaches, individual radiosonde measurements, and statistics against global circulation analyses from the NCEP and ECMWF. It is shown that thin layers of significant moisture variability can be detected, and that atmospheric water profiles can be retrieved even in cases where the ancillary data are not optimal.

1. Introduction

Water vapor is the dominant greenhouse gas in the atmosphere. However, measuring its global distribution and dynamics remains a challenge to remote sensing techniques, and Global Circulation weather analyses show significant discrepancies from the data [e.g. *Fasullo & Sun,* 2001]. Besides quantifying the global distribution of water in the atmosphere, it is important to understand its role in different climate processes. Thin cloud layers at high altitudes are difficult to detect and yet play an important role in the chemical and radiative properties of the upper troposphere and lower stratosphere. Proper characterization of such structures is necessary to improve our current understanding of the impact of this region in climate where the radiative properties of water modulate the response of the atmosphere to solar forcing. This factor is crucial for the assessment and prediction of the impacts of global change where an adequate knowledge of the diabatic processes in the atmosphere remains a challenge [e.g. *Goody,* 2001].

Different sounding techniques are able to extract certain aspects of the atmospheric water distribution which are complementary to each other. Atmospheric radio occultations provide vertical profiles of the atmospheric refraction index, n, with high vertical resolution [*Kursinski et al.,* 2000; *Anthes et al.,* 2000; *Gorbunov,* 2001; *Hajj et al.,* 2002, and references therein]. This refraction index can be used to extract specific humidity profiles either directly or indirectly. The high vertical resolution of occultations makes it a candidate to capturing vertical moisture and temperature structures not resolved by weather analyses and other remote

Paper number 2002jd002880.
0148-0227/03/2002jd002880$9.00

sensing techniques. Such fine scale moisture and temperature profiles can be used to detect clouds using methods as discussed e.g. in *Wang et al.,* 2000 and other references therein. The remote sensing character of radio occultations from a receiver aboard a satellite enables global coverage, offering information on weather processes in remote areas not easily accessible to other instruments of high vertical resolution such as radiosondes.

Current standard retrieval techniques require previous knowledge of atmospheric temperature profiles to infer atmospheric water content from radio occultation measurements. Temperature profiles derived from global weather analyses have proven to return very accurate results [*Anthes et al.,* 2000; *Kursinski & Hajj,* 2000], however some limitations have been detected that are addressed in this work. A significant fraction of the occultation retrievals, between 20% and 30%, seems to detect inconsistencies between the occultation profiles and the weather analyses. In these retrievals, when the temperature field from the analysis is combined with the measured refraction index profile, negative values of water vapor pressure are predicted. This fact is typically understood as a sign that the model profile does not represent appropriate ancillary data for the measured occultation profile. This type of inconsistency is a dominant source of water vapor retrieval inaccuracy for radio occultations. The current work explores the capabilities of radio occultations for independent profiling of atmospheric moisture, and describes preliminary results of a novel approach to estimating atmospheric water vapor. This novel approach does not rely on weather analyses and may overcome the current limitations. Its capabilities and current inaccuracies are discussed.

1.1. Technical background:

The atmospheric radio occultations described in this work are active limb soundings in which a receiver tracks the coherent signal broadcast by the Global Positioning System (GPS) satellites as they occult or rise behind the Earth's atmosphere. The GPS satellites transmit a coherent radio signal at two carrier frequencies, $L_1 = 1,575.42$ MHz and $L_2 = 1,227.6$ MHz, which are not absorbed by water, thus penetrating through clouds. As the GPS signals traverse the atmosphere, they are bent by the atmospheric density gradients across the ray path and this bending introduces a delay in the phase of the signal that can be measured [*Kursinski et al.,* 2000, and references therein]. The rate at which the delay changes can be used to calculate the bending, α, of the signal as a function of the ray impact parameter, a. The impact parameter is defined as the perpendicular distance between the center of the local ray curvature near the tangent point of the ray and the asymptotic straight line followed by the ray as it approaches the atmosphere. For an atmosphere which is locally spherically symmetric, there is a unique relationship between the bending $\alpha(a)$ and the atmospheric refractive index $n(r)$, such that the bending can be used, in turn, to derive $n(r)$ along the atmospheric layer traversed by the ray. During an occultation, GPS signals are tracked which traverse the atmosphere at different heights. Vertical profiles of bending angle are obtained with a vertical resolution equal to or less than the Fresnel diffraction limit, which ranges typically from 100 m to 1000 m for receivers on Low Earth Orbiters and less for receivers within the atmosphere. This vertical resolution can be improved with different wave

optics techniques discussed in *Gorbunov* [2001]. The resulting refraction index profiles have higher vertical resolution than any other remote sounding technique.

1.2. Atmospheric variables and radio-refractivity:

In radio occultations the refraction index is expressed in terms of the refractivity N. Refractivity is defined as one million times the deviation of a medium's refractive index from vacuum, $N = (n-1)\times 10^6$. For radio waves within the atmosphere N relates to pressure and temperature through:

$$N = a_1 \frac{p}{Z_d T} + a_2 \frac{e}{Z_w T} + a_3 \frac{e}{Z_w T^2} \quad (1)$$

[*Thayer,* 1974; *Bevis et al.,* 1994], where T is temperature in Kelvin, $p = p_d + e$ is total pressure in millibar, p_d is partial pressure of the dry component of air, e is water vapor pressure in millibar, $a_1 = 77.6$ K/hPa, $a_2 = -12.81$ K/hPa [*Thayer,* 1974] ($a_2 = 0$ following *Smith & Weintraub,* [1953]; $a_2 = -7.2$ following *Bevis et al.,* [1994]), $a_3 = 3.776 \times 10^5$ K^2/hPa [*Thayer,* 1974; *Smith & Weintraub,* 1953] ($a_3 = 3.739\times 10^5$ following *Bevis et al.,* [1994]), and Z_d and Z_w are the compressibility factors that account for non-ideal gas effects on air. The compressibility factors are considered unity in *Bevis et al.,* [1994] and throughout this work. Figure 1 shows the difference between the different coefficient values found in the literature and the effect of considering the compressibility factor equal to unity for a standard atmosphere with saturated water vapor content. This figure sets upper bounds to the errors in the formula. When compressibility factors are set to one, the difference between all expressions is at the per-mil level as seen in figure 1.

Figure 1.

Figure 1

Water vapor follows a conservation law: specific humidity, q, remains constant in the absence of sources or sinks of moisture. Examples of sources are processes such as evaporation, or moisture diffusion and transport by contact with a wet front. Sinks occur in the case of precipitation or mass exchange with a dry front. It will prove useful to exploit this conservation law and express refractivity changes in relation to deviations from a conserved q. For an ideal gas, $p_d = R_d \rho_d T$, and $e = R_w \rho_w T$, where $R_d = R/m_d = 287$ is the universal gas constant divided by m_d, the molecular mass for air, $R_w = R/m_w = 462$ is the gas constant divided by m_w, the molecular mass for water vapor, ρ_d is the density of the dry air component, and ρ_w is the density of water vapor. The ratio between wet and total density, $\rho = \rho_d + \rho_w$, defines the specific humidity through $q \doteq \frac{\rho_w}{\rho_d+\rho_w} = \frac{1}{\frac{R_w}{R_d}\frac{p_d}{e}+1}$. Refractivity can now be written in terms of specific humidity, temperature and density as:

$$N = a_1 R_d \left[1 + \left(\frac{R_w}{R_d} - 1 + \frac{a_2 R_w}{a_1 R_d} + \frac{a_3 R_w}{a_1 R_d}\frac{1}{T}\right) q\right] \rho \quad (2)$$

To understand the relative magnitude of the terms in the previous expression, one can separate the contributions to refractivity into the following terms: $k_1 = R_w/R_d - 1 = 0.6098$, which is the contribution to the total pressure term in equation 1 due to the changes in molecular weight of air associated with changes in its moisture content, e; $k_2 = (a_2 R_w)/(a_1 R_d) = 0.1494$ which is the contribution by the e/T term in eq. 1 and; $k_3 = (a_3 R_w)/(a_1 R_d) = 7756.29$.

Since water is typically retrieved at temperatures higher than 250 K, the dominant contribution from moist air to equation 2 comes from k_3, through k_3/T, and ranges from 31 in the upper troposphere to 26 in the lower troposphere. Specific humidity values are typically $q < 20 \times 10^{-3}$ near the Earth's surface. Thus, an upper bound to the contribution by the moist component of air to eq. 2 is around 52% of the dry component. For typical moist content values in the upper troposphere and the stratosphere (a few parts per million), the dominant wet contribution comes down to about 0.052% of the dry component. This contribution is undetectable from direct measurements of refractivity since the errors in the retrieved refractivities are estimated to be between 0.2% and 1% of N below 40 km and between 1% and 10% from 40km to 60 km height [e.g. *Kursinski et al.,* 2000]. The accuracy of eq. 1 using the correct compressibility factors, is predicted to have typical errors of 0.04% at 500 hPa, 0.1% for high humidities at low altitudes [*Thayer,* 1974], and it is further constrained when using the other expressions discussed in *Bevis et al.* [1994] as is illustrated in figure 1.

2. A simple model of atmospheric refractivity:

The main difficulty in extracting information about atmospheric moisture from eq. 2 is our incomplete knowledge of the physics of atmospheric water vapor. Equation 2 is one relation with three unknowns p, T, and e, and hence is undetermined without two additional equations. If enough physical constraints could be established linking temperature, density and water content in the atmosphere, they would provide a complete set of relations to extract the three variables from a given refractivity profile. But the atmosphere is a nonlinear open system constantly driven out of thermodynamic equilibrium by diabatic processes. Therefore, even though the laws of water vapor may be known, the final relations between atmospheric moisture content and the other thermodynamic variables is not direct.

At high altitudes where water content is undetectable, $q = 0$, atmospheric refractivity is directly proportional to density (see equation 2), and hydrostatic balance combined with the ideal gas law enables one to obtain pressure and temperature profiles [e.g. *Hajj et al.,* 2002]. Hydrostatic balance, $\partial_z p = -\rho g$, is one constraint relating density to pressure changes and determines the retrieval problem in dry regions of the atmosphere. The retrievals obtained are very accurate even in situations when slightly slanted rather than vertical layers of the atmosphere are scanned [e.g. *Anthes et al.,* 2000], or when non-hydrostatic effects may be sizeable. For instance, gravity waves reflect deviations from local hydrostatic equilibrium [e.g. *Houghton,* 1986; *Holton,* 1992], yet GPS radio occultations have provided accurate measurements of the temperature variances associated with gravity waves [*Preusse et al.,* 2000].

Direct inspection of eq. 2 shows that if specific humidity remained constant as a function of height, refractivity would change according to the laws followed by density and density over temperature. Atmospheric density follows closely an exponential dependence on height, and it is straightforward to show that in an ideal gas in hydrostatic balance with a constant temperature lapse rate, density over temperature is proportional to the vertical derivative of density, and thus close to another exponential. Refractivity will therefore be

nearly exponential for an atmosphere with constant specific humidity. However, because of the large k_3 factor, small changes in specific humidity will be largely amplified compared to what an exponential would do. The core idea of the method described here is therefore to match atmospheric refractivity and density to a local exponential law (within vertical segments slightly larger than one kilometer) and then assume that the deviations from the exponential law measured by the occultation are caused predominantly by the changes in water vapor. Such deviations are then used to estimate the changes in specific humidity with height.

In a spherically symmetric moist troposphere in hydrostatic balance, under the ideal gas assumption, constant lapse rate, $\Gamma \doteq -\partial_z T$, and constant specific humidity, density would follow the power law:

$$\frac{\rho(z)}{\rho(z_o)} = \left[1 - \frac{\Gamma}{T(z_o)}(z - z_o)\right]^{-B} \tag{3}$$

where $B \doteq 1 - \dfrac{g}{\Gamma R_d \left[1 + q\left(R_w/R_d - 1\right)\right]}$. For height differences $(z - z_o) \sim 1 - 2$ km, typical tropospheric values of $\Gamma < 8$ K/km, and $T > 250$ K, imply that the second term is very small. A Taylor expansion of the logarithm of eq. 3 leads to:

$$\log \frac{\rho(z)}{\rho(z_o)} = B\left[\frac{\Gamma(z - z_o)}{T(z_o)} + \frac{\Gamma^2(z - z_o)^2}{2T^2(z_o)} + O\left(\frac{\Gamma(z - z_o)}{T(z_o)}\right)^3\right]$$

The first term of this Taylor expansion corresponds to an exponential. The second is less than 1.5 - 3.2% of the first term if z is taken at distances of 1 to 2 km from z_o. In our local approach, z_o is chosen at the nearest point to the extrapolation point z. This distance is typically 0.8 km or less in the troposphere and the upper bound for the correction in the second term is of the order of 1% of the first or less. These corrections compare favorably with the differences shown in figure 1.

During an occultation refractivity changes captured between 2 consecutive measurement points are given by $\Delta N = \int_t^{t+\Delta t} dN = \int_t^{t+\Delta t}(\partial_x N \cdot dx + \partial_y N \cdot dy + \partial_z N \cdot dz + \partial_t N \cdot dt)$, that is, $\Delta N = \int_t^{t+\Delta t}(\partial_x N \cdot dx + \partial_y N \cdot dy + \partial_z N \cdot dz) + N(x, y, z, t + \Delta t) - N(x, y, z, t)$, where Δt is the time between one measurement and the next. For a spherically symmetrical atmosphere, or for one in which N represents a horizontal average, $\Delta N = \int_t^{t+\Delta t} \partial_z N \cdot dz + N(x, y, z, t + \Delta t) - N(x, y, z, t)$. Only the integral term, describing the vertical variability, will contribute. This is so because typical occultation sounding times are of the order of $\Delta t = 0.02$ seconds between two data points, while the change in atmospheric refractivity within such time intervals is given by the length scale between consecutive measurements, 100-1000 m, divided by the fastest possible speed for changes of the atmospheric state. An upper bound for the speed of atmospheric changes is the speed of sound. Therefore, changes of atmospheric refractivity gradient at one location occur at time scales longer than 1/3.6 sec which is much larger than $\Delta t \sim 0.02$ sec. By similar arguments, only the vertical variability of the thermodynamic variables p, T, q will be considered.

2.1. Extracting atmospheric moisture profiles

As mentioned above, the key idea is to infer a law for refractivity under the condition of constant specific humidity. This is done by fitting density to the Taylor expansion of its power law in eq. 3 for a set of points within a vertical distance of 1 km. The resulting fit is used to predict the density at the level immediately below that 1 km window. The refractivity related to that extrapolated density is then calculated. The difference between this extrapolated refractivity and the measured refractivity is assumed to be dominated by the effects of changes in specific humidity. A detailed description of how such changes are modeled follows in this subsection.

A fit is started from the upper atmosphere, where the air can be considered dry until the lowest point where the temperature lapse-rate reaches 2 K/km. A fit to the measured refractivity starts at the level immediately below this point. At these heights the temperature is too cold and the current noise level in refractivity retrievals is larger than the contribution of water content to eq. 1. The atmosphere is therefore considered dry for the first fit within 1 km below the tropopause. The coefficients of the Taylor expansion for the density power law are obtained by least-squares fit of the data to:

$$\log \frac{\rho(z)}{\rho(z_o)} = c_0 + c_1(z - z_o) \tag{4}$$

where c_1 stands for the first contribution in the Taylor expansion of eq. 3, and c_0 partially represents the nonlinear contributions. Higher order fits including the non-linear terms were tried but they were observed to produce unphysically large specific humidities. This may be a consequence of non-linear amplification of errors by the non-linear terms in the extrapolation step. Inclusion of the non-linear terms may need a different type of numerical strategy. Representing the nonlinear contributions by a constant c_0 prevented the amplification of such errors. The actual values extrapolated in these fits showed typical refractivity differences of less than 0.5% with the observation values.

The causes of refractivity changes from one occultation height level to the next are twofold. The first cause is the change associated with the change of density and temperature with height, while the second is related to possible changes in specific humidity. One can thus understand the refractivity changes between two consecutive heights, z and $z + \Delta z$, as:

$$N(z + \Delta z, q + \Delta q) = N(z, q) + \left(\frac{\partial N}{\partial z}\right)_q \Delta z + \left(\frac{\partial N}{\partial q}\right)_{z+\Delta z} \Delta q \tag{5}$$

The fit to eq. 4 and a linear temperature extrapolation are used to predict the contribution to refractivity changes with height in eq. 5. The difference between the observed refractivity and the fit-based prediction is identified thereafter with the last term in eq. 5. The changes in specific humidity that are not captured by the extrapolation law and have not been accounted for in any of the previous expressions are discussed next.

The analytical estimate of the first incremental change in

eq. 5 can be evaluated by subtracting eq. 2 at two different heights assuming constant q as:

$$\left(\frac{\partial N}{\partial z}\right)_q \Delta z =$$

$$a_1 R_d \left\{ \left[1 + q \cdot (k_1 + k_2)\right] \Delta\rho + k_3 \left[\frac{\rho(z+\Delta z)}{T(z+\Delta z)} - \frac{\rho(z)}{T(z)}\right] \right\} \tag{6}$$

where $T(z+\Delta z) = T + \Delta T = T(z) - \Gamma \Delta z$, $\Delta\rho = \rho(z + \Delta z) - \rho(z)$, $q = q(z)$, $\Delta z < 0$, with the values of density obtained from the extrapolation of the fit within a window 1 km above z, extrapolated to $z+\Delta z$, and temperature lapse rate assumed constant within the nearest 2 neighbors of the value at z.

The difference between the measured refractivity increment, $N(z + \Delta z, q + \Delta q) - N(z, q)$, and eq. 6 is identified with the last term in eq. 5. Using the incremental change of eq. 2 with q at constant temperature and density, one has the identity:

$$\left(\frac{\partial N}{\partial q}\right)_{z+\Delta z} \Delta q =$$

$$a_1 R_d \left(k_1 + k_2 + \frac{k_3}{T + \Delta T}\right) \left[\rho(z+\Delta z) + \left(\frac{\partial \rho}{\partial q}\right)_{z+\Delta z}\right] \Delta q \tag{7}$$

Changes of density with moist content, $\partial_q \rho(z + \Delta z)$, are modeled assuming that they are caused only by a change in internal composition of the parcel of air that occupies the unit of volume. Such a change means that each mole of dry air is exchanged with a mole of wet air on a one to one basis, and that the changes in the associated molecular masses account for the changes in density. This is equivalent to assuming locally non-divergent air flow. A loss or gain of wet molecules will produce a change in pressure with respect to the environment. The environment will try to reach pressure balance by filling the vacuum in case of a loss, or ejecting molecules in case of a gain. To reach the pressure of the environment the adjustment in partial pressures follows Dalton's law. The physical mechanisms behind this process will be a combination of winds and slow diffusion. The expression for that contribution is thus (see Appendix):

$$\left(\frac{\partial \rho}{\partial q}\right)_{z+\Delta z} \Delta q = \left(1 - \frac{R_w}{R_d}\right) \frac{\rho \Delta q}{(1-q) + q\frac{R_w}{R_d}} \tag{8}$$

Substitution into eq. 7 yields

$$\left(\frac{\partial N}{\partial q}\right)_{z+\Delta z} \Delta q =$$

$$R_d a_1 \left[k_1 \left(1 - \frac{1}{1 + k_1 q}\right) + k_2 + \frac{k_3}{T + \Delta T}\right] \rho \Delta q \tag{9}$$

One can see that the correction introduced by using Dalton's law is a term of typically less than 1% of the main contribution k_3, but comparisons with radiosonde profiles showed that including this term yields better results than neglecting it. This final expression, when identified with the difference between the measurement and the refractivity increment predicted by eq 6, leads to a Δq. To initialize q at the top boundary two approaches were tried $q = 0$

and the saturation value for the temperature at that initialization height. The best statistical results where obtained when initialization occurred with the saturation value, and are therefore the only ones discussed here.

For the sake of totally freeing up the retrieval from model input, temperature initialization needed at the top was also done on occasion by using an exponential fit to the uppermost three values. Statistical comparisons of such temperature initializations made at 50 km, showed sub-Kelvin differences with the retrievals made with standard model initialization below 30 km. Individual cases of such temperature initializations, as well as other approaches that led to less successful water vapor retrievals, are discussed elsewhere in detail [*Nilsson,* 2002].

3. Results

Two sets of comparisons were made. The first group was with 114 nearby, radiosonde measurements, less than 12 hours and 1 degree latitude and longitude apart. The second group of comparisons was made with profiles from the NCEP model that had a refractivity very close, less than 10% difference, to the occultation retrieval.

Figure 2.

Figure 2

Radiosonde measurements have a high vertical resolution that can be used to validate the ability of occultations to capture the fine-scale structure of atmospheric moisture profiles. Figures 2 illustrate the capability of occultations to detect moisture profiles which are not captured by the NCEP analysis (grey line), but are present in the radiosonde measurement (thick dashed black line). Figure 2a shows an occultation where a moist structure is captured near 6.5 km which escapes the model from NCEP. This occultation was chosen because it also illustrates a common problem with the current processing technique (squares) which yields negative moisture values 20%-30% of the times. Figure 2c shows another case in which all methods, radiosonde (thick dashed black line), model (grey line) and the occultation retrievals capture a moist structure below 8 km. The current processing method, however, shows a sudden jump in the moisture content. This jump is caused by the fact that moisture is accounted for only at heights below the level where temperature is warmer than 250 K. If the model and occultation values are somewhat inconsistent with each other, the standard retrieval's efforts to match refractivity with the model prediction may lead to this type of spurious behavior. Note that the source of the error is possibly in a model refractivity which is not consistent with the observation. As a consequence, the retrieval based in the fitting technique described in this work does not show such model induced jumps. In both figures, this work is closer to the radiosonde measurement than the current retrieval technique.

Figure 3.

Figure 3

The fitting technique described here is expected to cause errors whenever the leading assumptions break down. This occurs for example in the case of atmospheric waves that cause deviations from hydrostatic balance, or for sharply nonlinear temperature profiles within the 1 km fitting windows. Figures 3a and 3c illustrate the error observed under such circumstances. Figures 3b and 3d show the corresponding temperature profiles according to a dry retrieval (water vapor is assumed to be zero), the NCEP and ECMWF analyses, and to nearby radiosondes. Figures 3 show two ex-

ceptional cases where the model-free method dramatically underperformed the others. Both cases correlated with a sharp deviation from a linear temperature profile. A green line has been added to show the model free water vapor estimates if T were considered constant and equal to 280 K in eqs. 6 and 9. The constant T results are close to the results with the model profile, which captures the oscillations in temperature. This suggests that the source of the error in q is not in the temperature values, but in assuming that deviations from an exponential refractivity profile are solely caused by moisture changes when the temperature profile is locally nonlinear. Figures 3a-b show a measurement off the coast of Japan at 38.3N 141E in which the specific humidity displays a physically improbable bulge between 10 and 4 km. This characteristic shape with moisture content much higher in the upper than in the lower troposphere is easy to identify as an unlikely situation since water vapor content typically decreases with altitude. A nonlinear temperature profile with a fine scale bulge was captured, besides, by the dry retrieval, the radiosonde, and the analyses between 11 km and 4 km. Figures 3c-d show a situation in which water vapor is underestimated at the bottom. In this case only the temperature profile captured by the dry retrieval is again associated with a wavy structure in the temperature profile between 5.5 km and 3.5 km. The fact that the dry retrieval captures such sharp temperature structures sets a model-independent criterion to identify cases where the fitting procedure may yield poor water vapor retrievals. In general temperature profiles remain close to linear in the troposphere within the one kilometer windows used leading to better agreements. Despite the quantitative disagreement in 3c, the shape of the moisture profile still ressembles the standard occultation retrieval.

Note that in the method proposed here the coefficients of the fits to an exponential are updated after each kilometer segment. This is equivalent to requiring a constant lapse rate only within such a segment and does not require the whole troposphere to keep a constant lapse rate. Therefore this method also works for temperature profiles that are nonlinear, as in Figure 2d which has a smoothly nonlinear lapse rate.

While qualitative agreement has been found, quantitative validations are difficult. Radiosonde measurements are very local compared to the typical 200-300 km horizontal averaging scale of occultation measurements. Moist structures of small horizontal extent will therefore be averaged out. This sets constraints upon the representativity of direct comparisons between both observational methods. Besides, occultation and radiosonde measurements might not be coincident in time. A few cases were found, out of 114 comparisons, in which there were radiosonde measurements few hours before and after the occultation. In all such cases observed, the moisture profile captured by the consecutive radiosondes changed with time by an amount which was comparable or larger than the difference between the radiosonde and the occultation results.

Table 1

Table 1

Although the previous comparisons show qualitative agreement, a statistical quantitative comparison was done with output from the NCEP analysis interpolated to the location and time of the occultation's tangent point as well. To validate the new retrieved profiles, the comparison had to be made between cases where model and observation were

capturing consistently the atmospheric state, 2000 occultations from the SAC-C satellite and 2000 from CHAMP were scanned from the months of August and September 2001. Out of these, 3202, 80 %, captured refractivity differences between model and observation of less than 10% at all heights, and the temperature obtained in solving eq. 1 when assuming water vapor from the NCEP model as the correct value of p_w differed by less than 10K from the occultation temperature at all heights above 2 km. Profiles filtered out correspond thus to either model or retrieval errors. The selection ensured that the model prediction is appropriate for validation of the observation values. Of these selected 3202 occultations, 746, about 23%, still led to negative water vapor pressure values at some heights when the temperature from NCEP was assumed correct and substituted into eq. 1 for the standard processing. The mean and standard deviation of the differences with NCEP and the fit procedure are shown in Figure 4 as a function of pressure to enable easy comparison with a previous attempt to infer water vapor without using models [*O'Sullivan et al.,* 2000]. Figure 4a shows the 2466 cases where water vapor pressure remained positive at all heights after combining NCEP's temperature and the observed refractivity in eq. 1. Figure 4b corresponds to the 746 cases where some values became negative. In both figures, the mean difference with the NCEP prediction is represented by a symbol, the error bar spans from the mean difference minus the standard deviation to the mean difference plus the standard deviation. The statistics reflect mean value and deviation for the values within bins spanning over ranges of 50 hPa. Green circles show the results with the standard occultation processing, red squares represent the fit approach using a linear lapse rate in eq. 6 based on NCEP temperatures and eq. 9 to extrapolate the temperature values. Open circles illustrate the results if the temperature is assumed constant in eq. 6 and 9 throughout the whole troposphere with a value of T =280K.

Figure 4.

Figure 4

Several results are apparent from figures 4. First is the fact that both figures show a smaller mean difference and standard deviation than a previous effort to retrieve water vapor from occultation refractivities without using the model in *O'Sullivan* [2000]. A second advantage is that that previous work required ancillary data at the ground level, which prevents its global use above the ocean according to the authors. The fitting method described here does not require values at ground level and yet appears closer to the NCEP analysis. Second, that the standard processing technique provides a more accurate result than the method described here when NCEP captures the ratio between dry and wet contributions to refractivity consistently with the occultation results and no negative specific humidities are obtained. Figure 4b on the other hand shows that our fit technique outperforms the current processing in comparisons with NCEP by having a smaller difference in the mean and standard deviation at all heights above 900 hPa. In both figures, the mean differences are of comparable magnitude and smaller than the standard deviations. Standard deviations are also influenced by refractivity biases at low altitudes, and by the fact that small scale variability, which is not captured by the model, is being captured by the occultation. Thus the exact size of the standard deviations is not as important as the fact that they have similar magnitudes when using the standard retrieval or the fitting method.

The occultations in Figure 4b indicate problems with the NCEP model, and therefore a validation was made against interpolations of ECMWF to the occultation times and tangent points. These comparisons are shown in Figure 4c for 402 occultations. It is seen that the mean difference between NCEP and ECMWF (red squares) is smaller but compares to the differences between the fitting method and ECMWF (open circles) under 900 hPa. Above 900 hPa the mean result from the occultation is closer to ECMWF than the NCEP model results. Figure 4c also shows the difference between using ECMWF as ancillary data for the standard occultation retrieval or using NCEP. The differences between the models in Figure 4c are larger than the differences between the fit results for the occultation and ECMWF. Finally, the fit method is not very sensitive to errors in the retrieved temperature, since retrievals with constant T=280 K did not differ significantly from the others which used the temperature from the model.

In comparing results from fitting to 1 km and 2 km windows with the NCEP analysis, 1 km windows returned better statistics. This can be understood from the discussion about the error involved in assuming an exponential atmosphere instead of eq. 3. Initialization of specific humidity to be the saturated value rather than zero at the first interval led to slight improvements in the statistics in general. The improvements were noticeable when there were moisture structures in the upper troposphere. In such cases, underestimating the initial q led to a zero q at some heights, and an overestimate of density below.

4. Summary and conclusions

It has been shown that simple physical principles may be used to estimate water vapor in radio occultation soundings of the atmosphere. The preliminary results discussed here offer a start to a new type of retrieval approaches. Convective adjustment parameterizations, non hydrostatic corrections like those induced by waves, thermodynamic constraints (like the relation that the Clausius Clapeyron law sets on temperature changes with moisture increments) were not included. Improvements are expected as more of these physical constraints are included. The incorporation of iterative mathematical algorithms, or optimal estimation techniques promise additional improvement. Such considerations will also lead to establishing absolute error bars for the method and should be our next step.

Despite using a simple model, the preliminary results shown in this work already compare favorably with related previous works, and are reasonably close to the current standard retrievals which rely on weather analyses. Figures 4a,b, & c show that the statistics of the new method are comparable to the current radio-occultation approach when the water vapor pressure is forced negative due to presumed errors in the analyses (about 25%-30% of the occultations.) Comparisons with radiosondes illustrated in figures 2 show that the new method can provide valuable qualitative information on the location of thin moisture layers in the upper troposphere ($T < 250$ K), where their role is crucial for understanding tropospheric-stratospheric exchange, heterogeneous chemistry in the lower stratosphere, and radiative properties of this region.

The results in Table 1 make a case for model independent techniques. The criteria used to select the occultations for

the statistical comparisons give an idea of the quality of current NCEP model predictions. Tropical occultations have been filtered out in 450 cases, proportionally more (32%) than at other latitudes. This singles out the largest differences between observation and the NCEP model at the tropics. Occultations in the Southern hemisphere failed the selection criteria in only about 13% of the cases, but the resulting profiles lead to inconsistent (negative q) results with the observation more frequently. This inconsistency reflects a model which captures refractivity values well, but which fails to capture correctly the relation of water vapor to temperature. Since the effect of negative water vapor would be to diminish refractivity at a given temperature, negative water vapor retrievals are indicative of a significant temperature error in the model profile. Northern latitudes failed the filtering criterion by about 12 % (similar to the Southern hemisphere), and lead to only 8% of cases with negative q. This is indicative of the model capturing better the results of the observations. There is no clear reason for this hemispheric asymmetry in Table 1, other than the fact that NCEP assimilates more data in the Northern hemisphere. If this is the cause, improved model independent water vapor retrievals from GPS radio occultations can help improve model predictions and parameterizations in the Southern Hemisphere and the Tropics where the dense coverage of radio occultations complement radiosonde data.

Acknowledgments. The authors want to acknowledge C.M. Roehl and F.H. Webb for carefully reading this manuscript, and useful discussions with G.A. Hajj, A.J. Mannucci. Funding for this work has been provided by NASA through the GEO, and GENESIS projects. The research described in this paper was carried out at the Jet Propulsion Laboratory/California Institute of Technology, under a contract with the National Aeronautics and Space Administration.of Technology,

Appendix: Derivation of $\partial_q \rho \cdot \Delta q$:

Density changes due to changes in atmospheric specific humidity are inferred from the following arguments. The density change due to a change in pressure with height is taken into account in the exponential extrapolation of ρ along the vertical. After that correction is considered, density in terms of particle density can be written

$$\rho = \frac{m^{tot}}{V} = \frac{n_d m_d + n_w m_w}{V} \tag{A-1}$$

where V is the volume occupied by a given parcel of air at a given pressure level if it has been moved down from another reference level keeping its composition (water content) constant; n_d and n_w are the number of moles of dry air and water; m_d, and m_w are their respective molecular masses. Mass transport in open systems is described by the continuity equation which states that, in the absence of sources or sinks of mass, the influx of particles into a unit of volume equals the outward flux of particles. This is equivalent to the requirement of non-divergence of air-flow. If wet air molecules are replaced by dry and vice versa:

$$\Delta n_d = -c\Delta n_w \doteq -\Delta n \tag{A2}$$

Taking $c \doteq 1$ yields

$$\Delta\rho = \frac{\Delta n_d m_d + \Delta n_w m_w}{V} = -\frac{m_d - m_w}{V}\Delta n \tag{A3}$$

From the definitions of specific humidity and Δn

$$q = \frac{\rho_w}{\rho} = \frac{n_w m_w}{n_d m_d + n_w m_w} = \frac{n_w m_w}{m^{tot}} \tag{A4}$$

$$1 - q = \frac{n_d m_d}{m^{tot}} \tag{A5}$$

$$\Delta q = \Delta n \frac{(n_d + n_w) m_d m_w}{(n_d m_d + n_w m_w)^2} \tag{A6}$$

Using this relation between Δq, Δn, and using that $m^{tot} = \rho V$

$$\Delta\rho = -\frac{m_d - m_w}{V}\Delta q \rho V \frac{m^{tot}}{m_d m_w (n_d + n_w)} \tag{A7}$$

Substituting for q and $1 - q$ yields the final expression

$$\Delta\rho = \left(\frac{m_w}{m_d} - 1\right) \frac{\rho \Delta q}{(1-q)\frac{m_w}{m_d} + q} \tag{A8}$$

which leads to the expression in (8).

References

Anthes, R. A., C. Rocken, and Y. -H. Kuo, Applications of cosmic to meteorology and climate. *Terrestrial Atmospheric and Oceanic Sciences*, *11,* 115–156, 2000.

Bevis, M., Businger, S., S. Chiswell, T. A. Herring, R. Anthes, C. Rocken, and R. H. Ware, GPS meteorology: Mapping zenith wet delays onto precipitable water. *Journal of Applied Meteorology*, *33,* 379–386, 1994.

Fasullo, J., and D.-Z. Sun, Radiative sensitivies to tropical water vapor under all-sky conditions. *J. Climate*, *14,* 2798-2807, 2001.

Gorbunov, M. E., Radioholographic methods for processing radio occultation data in multipath regions. *Technical report, Danish Meteorological Institute,* DMI, 2001.

Goody, R., Sources and sinks of climate entropy *Q. J. Roy. Meteor. Soc.*, *126,* 1953-1970, 2000.

Hajj, G., E. R. Kursinski, L. J. Romans, W. Bertiger, and S. S. Leroy, A technical description of atmospheric sounding by gps occultation. *Journal of Atmospheric and Solar-Terrestrial Physics*, *64,* 451–469, 2002.

Holton, J. R., *An Introduction to Dynamic Meteorology.* Academic Press Inc., San Diego, third edition, 1992.

Houghton, J. T., *The Physics of atmospheres.* Cambridge University Press, second edition, 1986.

Kursinski, E. R., and G. A. Hajj, A comparison of water vapor derived from gps occultations and global weather analyses, *Journal of Geophysical Research*, *106(D1),* 113–1138, 2001.

Kursinski, E. R., G. A. Hajj, S. S. Leroy, and B.M. Herman, The gps occultation technique. *Terrestrial Atmospheric and Oceanic Sciences*, *11,* 53–114, 2000.

Nilsson, M., Retrievals of water vapor using GPS radio occultations, Master Thesis, Department of Radio and Space Science, Onsala Space Observatory, Chalmers University of Technology, Sweden, 2002.

O'Sullivan, D. B., B. M. Herman, D. Feng, D. E. Flittner, and D. M. Ward, Retrievals of water vapor profiles from gps/met radio occultations. *Bulletin of the American Meteorological Society*, *81,* 1031–1040, 2000.

Preusse, P., S. D. Eckermann, and D. Offermann, Comparison of global distributions of zonal-mean gravity wave variance inferred from different satellite instruments. *Geophysical Research Letters*, *27,* 3877–3880, 2000.

Smith E.K., S. Weintraub, The constants in the equation for atmospheric refractive index at radio frequencies, *Proceedings of the Institute of Radio Engineers*, *41,*, 1035-1037, 1953.

Thayer, G. D., An improved ecuation for the radio refractive index of air. *Radio Science*, *9,* 803–807, 1974.

Wang, J., Rossow, W.B., Zhang, Y., Cloud Vertical Structure and Its Variations from a 20-Yr Global Rawinsonde Dataset. *Journal of Climate*, *13,* 3041–3056, 2000.

M. de la Torre Juárez, M/S 238-600, Jet Propulsion Laboratory/California Institute of Technology, 4800 Oak Grove Dr. Pasadena, CA 91109, U.S.A. (mtj@jpl.nasa.gov)

Mattias Nilsson Department of Radio and Space Science, Onsala Space Observatory, SE-439 92 Onsala, Sweden. (f96mani@dd.chalmers.se)

(Received 23 Aug. 2002; revised 13 Jan. 2003;
accepted 6 Feb. 2003.)

Table 1. Summary of water vapor retrievals for occultations with refractivities and temperatures that compare well with NCEP. The number of occultations filtered out because they differed by more than 10% in refractivity or 10K in temperature is also given in the parentheses.

Latitudes	Positive q	(filtered)	Negative q	(filtered)	Total
North[a]	1180	(119)	128	(72)	1499
Tropics[b]	722	(192)	255	(258)	1427
South[c]	564	(71)	363	(76)	1074

[a] North of 30 degrees N.
[b] Between 30S and 30N.
[c] South of 30 degrees S.

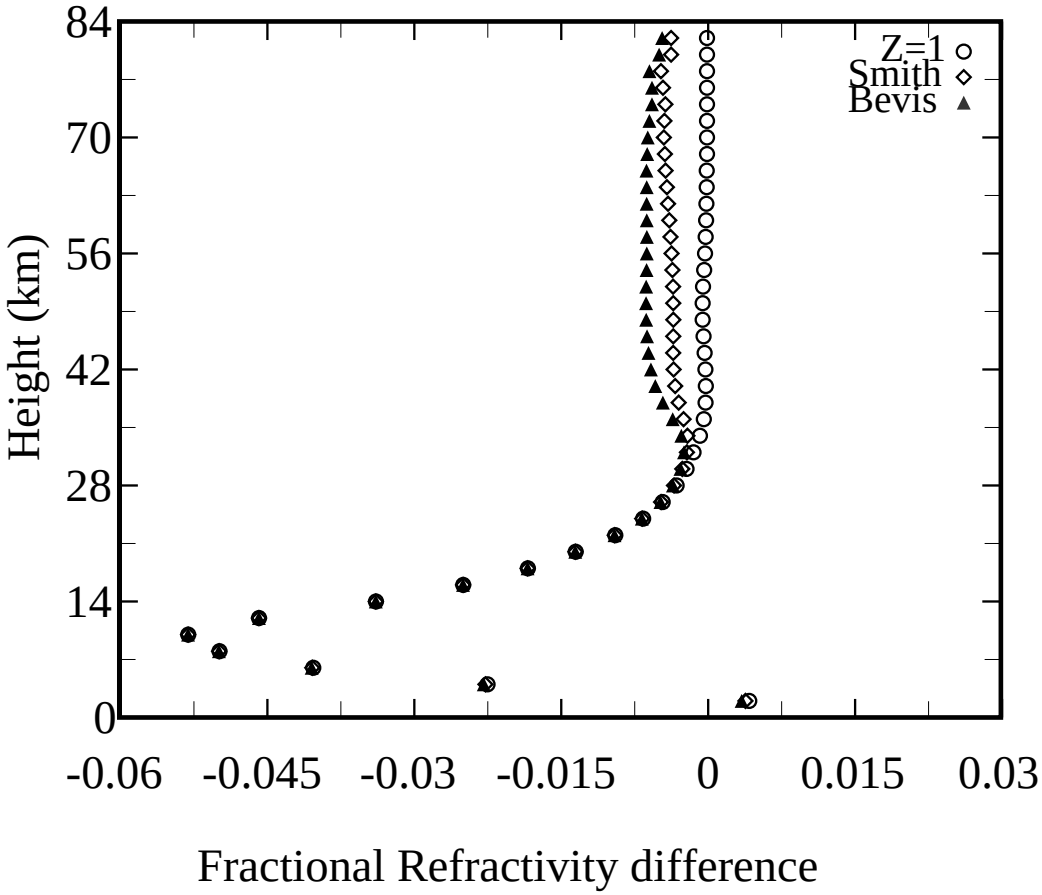

Figure 1. Differences between the full refractivity formula by *Thayer,* 1974, and: the same formula with compressibility factors $Z_d = Z_w = 1$; the coefficient values in *Bevis et al.,* 1994, and; the standard formula by *Smith and Weintraub,* 1953. The data correspond to a saturated atmosphere whose temperature and pressure matches the US Standard atmosphere.

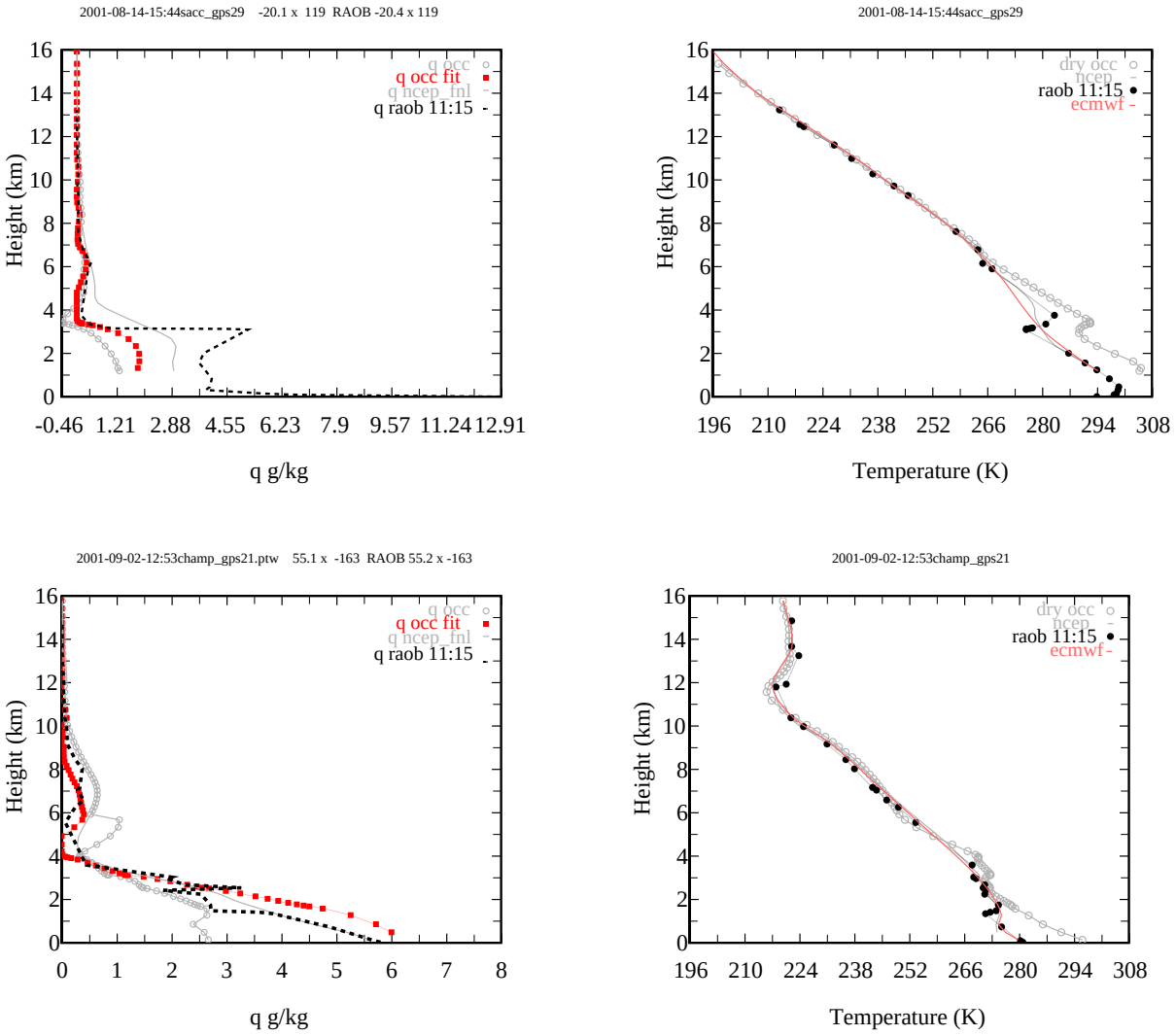

Figure 2. Top left to bottom right: a) Specific humidity versus height for a radiosonde (thick dashed black line), NCEP (grey line), standard occultation processing (red close squares) and the fitting procedure (grey circles). b) Temperature profiles corresponding to 2a according to dry occultation retrieval (grey circles), NCEP (grey line), ECMWF (orange), and radiosonde measurements (black symbols). c) Same as 2a for an occultation with negative water vapor pressures. d) Temperature profiles for 2c from dry retrieval, NCEP ECMWF, and radiosonde. The legends above the plots show year-month-day-hour:minute:seconds of the occultation, occulting receiver, latitude × longitude of the lowest tangent point, and latitude × longitude at which the radiosonde was launched. Radiosondes a and b were launched at 11:15 UTM.

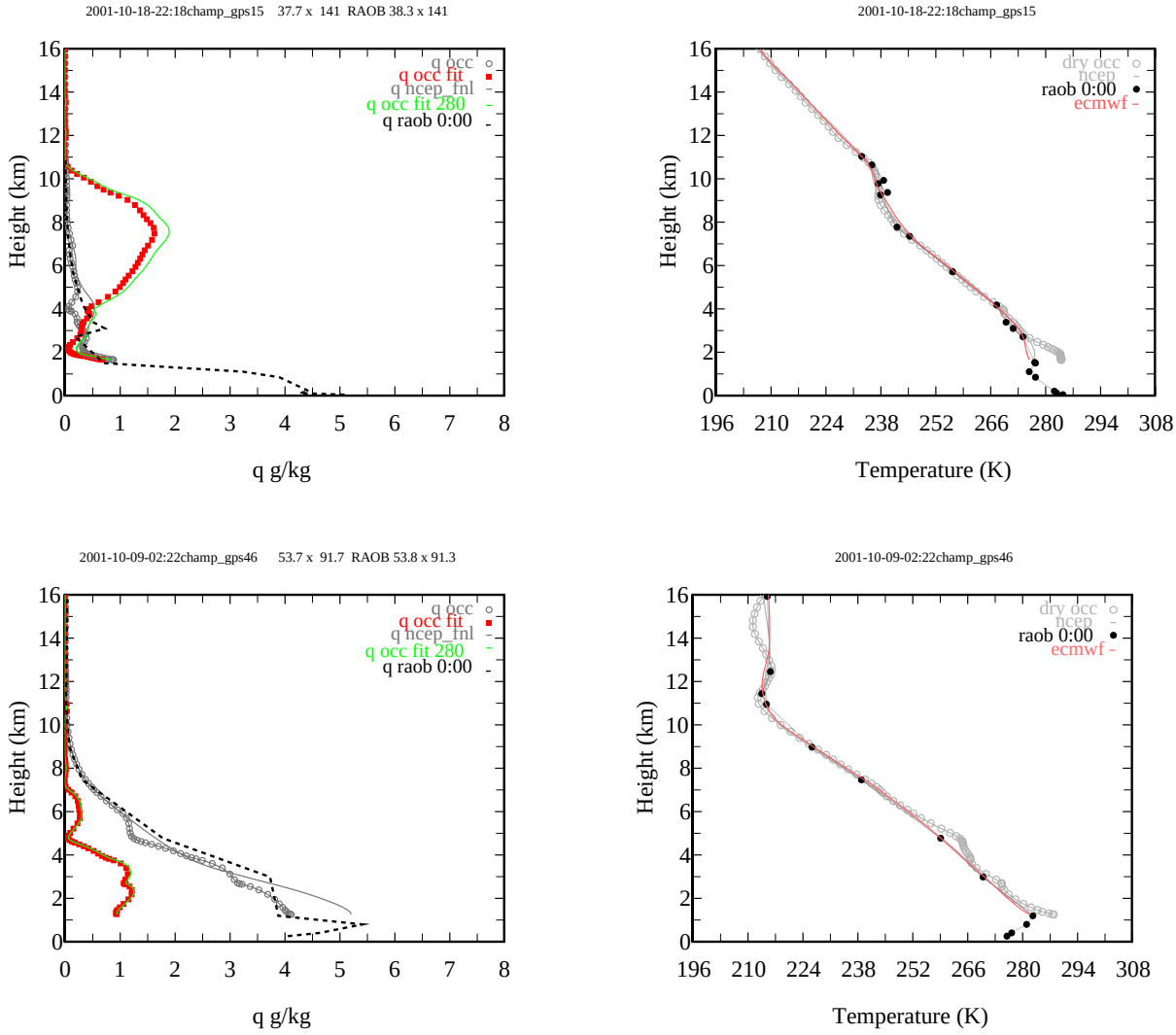

Figure 3. Top left to bottom right: a) The same as in figure 2a for an occultation where the fitting procedure fails above 8 km. A green solid line shows water vapor estimates with the fitting approach if T is taken constant and equal to 280. b) Temperature profiles corresponding to 3a according to NCEP (grey line), dry occultation retrieval (grey circles), ECMWF (orange) and radiosonde measurements (black symbols). c) Same as 3a for an occultation where the fit underestimates water vapor at all heights. d) Temperature profiles for 3c from NCEP, dry retrieval, ECMWF, and radiosonde. Both radiosondes were launched near midnight.

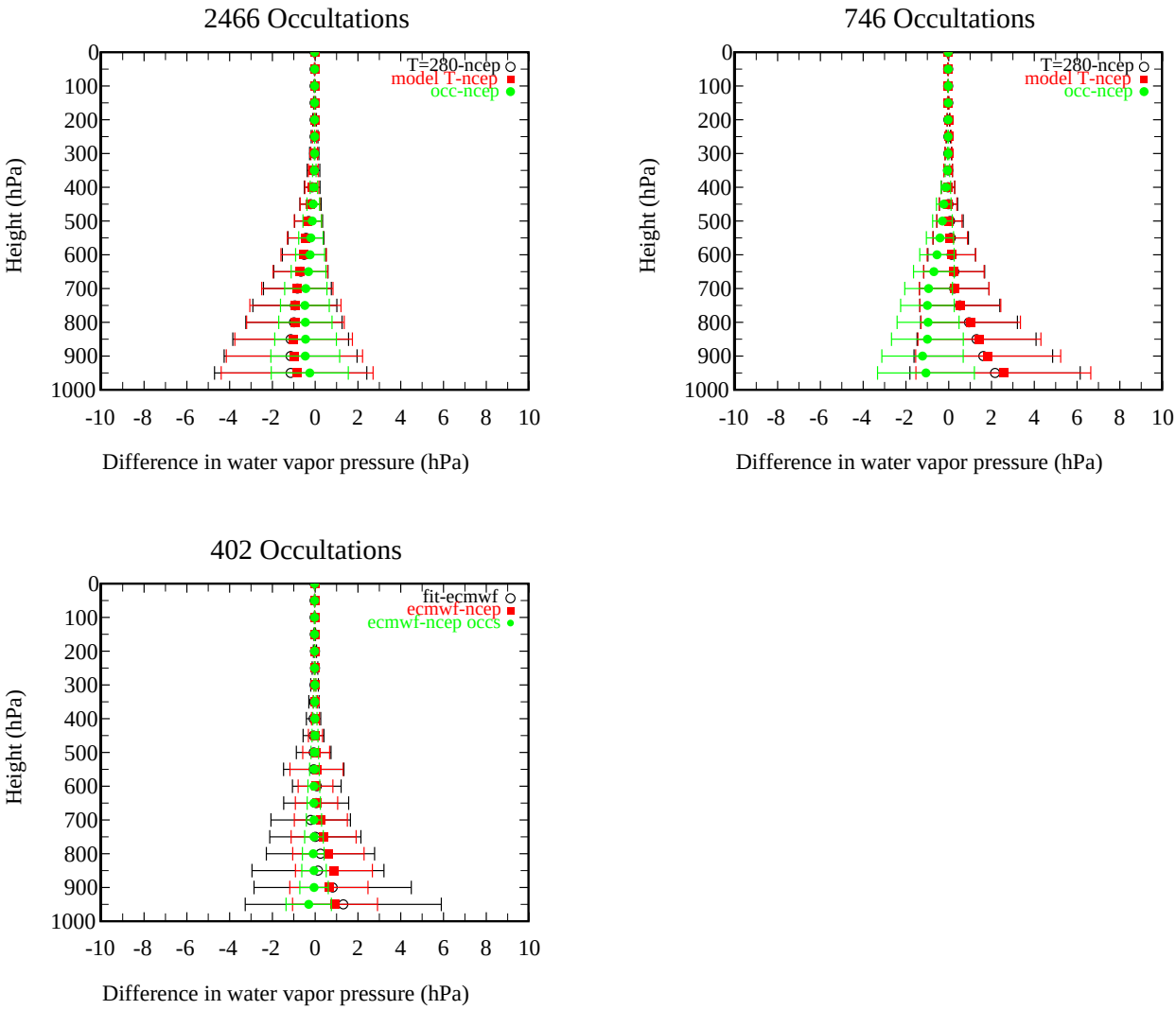

Figure 4. a) Top left. Statistics of the differences between the occultations with a positive water vapor pressure in the current processing and NCEP analysis predictions (green close circles). The same for the method described here when the temperature to calculate the lapse rates is taken from NCEP (red close squares) and when it is left constant at 280 K (black open circles). b) Top right. The same for the 746 occultations where the NCEP data would be consistent with the measured refractivity only if water vapor pressure is negative at some heights. c) Differences between ECMWF and NCEP (red close squares), occultations with ancillary data from ECMWF or NCEP (green close circles), and the method described here and ECMWF (open circles) for 402 of the occultations used in Figure 4b.